Scientific Research Publishing

Open Journal of Civil Engineering, 2022, 12, 271-291
https://www.scirp.org/journal/ojce
ISSN Online: 2164-3172
ISSN Print: 2164-3164

Using Geometry Data from Ground Penetrating Radar to Improve Pavement Layers Auscultation Using Seismic Surface Waves Inversion Method

Cheikh Diallo Diene, Mapathe Ndiaye

Laboratory of Mechanics and Soils Modelisation, University Iba Der Thiam of Thies, Thiès, Senegal
Email: Cheikhdiallo.diene@univ-thies.sn

How to cite this paper: Diene, C.D. and Ndiaye, M. (2022) Using Geometry Data from Ground Penetrating Radar to Improve Pavement Layers Auscultation Using Seismic Surface Waves Inversion Method. *Open Journal of Civil Engineering*, **12**, 271-291.
https://doi.org/10.4236/ojce.2022.123016

Received: May 20, 2022
Accepted: July 26, 2022
Published: July 29, 2022

Abstract

In order to reduce the unknown parameters during the inversion of the dispersion curve in the aim to obtain more precise Vs and V_P profiles, the Multi-Channel Analysis of Surface Waves (MASW) method was combined with the Ground Penetrating Radar (GPR) method. First, a 2D GPR profile was made on the pavement, then 1D MASW profiles spaced by 0.2 m apart in the perpendicular direction and centered on the intersection with the Radar profile. The GPR measurements, made with a 1600 Hz antenna, allowed to calculate the dielectric permittivities then velocities in order to convert the times profiles to depth. Thus, the thicknesses of the layers are directly read on the radar profile. MASW measurements were performed by simulating the Multi-Channel Simulation with One Receiver (MSOR) method in Land Streamer mode. Six 4.5 Hz pointless geophones are connected to the seismograph consisting of an Arduino Due microcontroller and a nano-computer type Raspberry Pi 4. The results of the dispersion analysis showed a fundamental mode located between approximately 70 Hz and 200 Hz and an inverted dispersion, characteristic of pavements with higher frequencies propagating at higher velocities. The results show that the integration of the number of layers and the thicknesses obtained from the GPR measurements in the inversion parameters makes it possible to obtain a more precise Vs and V_P velocity profile. All profiles, seismic and radar, have shown that velocities decrease with depth. The detected heterogeneities appear to be related to differences in water content inside the pavement.

Keywords

MASW, GPR, Auscultation, Route, Elastic Properties, Permittivity

1. Introduction

Pavement auscultation generally involves a series of more or less destructive tests which, in addition to information on the thicknesses of the different pavement layers, are designed to allow an assessment of the conditions of the materials and the quality of the interfaces. These tests with boreholes and cores are long and expensive and their number necessarily limited, which increases the uncertainty on the basic parameters. In addition, coring may damage the taken samples. Road engineers who have for a longtime wanted to inspect the pavement by transparency without destroying it can now do so using several tools such as the surface wave method and the GPR Radar method.

The first uses of surface waves in road auscultation were carried out by the German Soil Engineering Company (GSSM) [1]. Subsequently, Jones, Henklom and Klomp used steady-state vibrators to improve the method of surface waves on pavements [2]. In the early 1980s, several researchers worked on the development and application of the Spectral Analysis of Surface Waves (SASW) method on several pavements divided into flexible and rigid pavements [3] [4] [5], the results were then compared with other independent tests.

Subsequently, significant improvements were made and proved useful for roadside testing [6] [7] with the rise of Multi-Channel Analysis of Surface Waves (MASW) [8] [9] and Multi-Channel Simulation with One Receiver (MSOR) [10] which provided accurate non-destructive estimates for the calculation of the top-layer module of bituminous concrete.

However, the use of the MASW method as a pavement investigation method remains tedious due to several implementation factors; This led to the use of peakless geophones with the Land Streamer acquisition technique [11] [12].

Other difficulties were observed because of the fundamental nature of wave propagation in stratified environments, where rigidity decreases with depth, which is the case with a pavement system. Sezawa (1938) was the first to report the abnormal behaviour of surface waves in this type of medium, and his speculative findings revealed some of the difficulties to come. Choi *et al.* (2018) later confirmed the possible existence of surface waves in this type of medium.

In recent years, GPR has been shown to be a valuable non-destructive tool for assessing the thickness of the pavement layer [13] [14] [15]. Even better, Emund *et al.*, (2010) conducted a cumulative study between the radar GPR and the MASW method to determine variations in thickness and modulus of pavement layers. At the end of this study, they showed that by using the AASHTO 1993 guide for the design of pavement structures, the difference in module and thickness between the data integrating the GPR results resulted in a difference of almost two inches (5.08 cm) in the required cover thickness. There are also correlations between relative permittivities and compaction parameters of pavement granular materials [16] [17].

The objective of our study is precisely to combine the MASW and GPR me-

thods in order to be able to integrate the thicknesses obtained by Radar auscultation in the model parameters during the inversion of the dispersion curve in order to reduce the unknowns and obtain an accurate and unique V_S and V_P profile.

To achieve these objectives, Radar and MASW measurements will be carried out on the same profile of a road using respectively a GSSI Structure Scan Radar tool and a seismograph specially designed for road testing [12]. The Radar acquisition gives an amplitude profile from which we can calculate the permittivities [18] and deduce the velocities. From the velocities, the axis of the times can be transformed into depth, which allows to know the thicknesses of the layers directly on the profile.

In this article, we will first discuss, some theoretical aspects on radar and surface waves and their use for road layer testing before moving on to experimental measurements and interpretation and finally to a comparative study

2. Ground Penetrating Radar

In order to perform a reliable and non-destructive mean for straightforward road quality control, the use of the GPR is a major asset. It is with this in mind that several researchers have studied backfill construction, in particular the existence of relationships between compaction parameters and dielectric properties [19] [20]. In 2020, the Regional Laboratory for the Road and Road Network evaluated the metrological performance of its Radar systems with a view to better specifying their field of application [21].

In the road field, measurements of the thickness of pavement layers and the detection of irregularities by means of radar were carried out [22]. Interface between bituminous and hydraulic layers of mixed pavement structures [23] was also studied. A further a procedure for the determination of bituminous pavement layer modules from curvimeter lift measurements associated with radar thickness measurements was developed [24]. Subsequently, many researchers [25] [26] reported success in using ground penetration radar (GPR) technology to measure the thickness of the soft pavement layer.

The average velocity of propagation of radar waves in a medium is given as:

$$v = \frac{3\times 10^8}{\sqrt{\varepsilon_r}} \tag{1}$$

where ε_r is the relative dielectric permittivity of the site propagation

The attenuation of radar waves in an environment is usually expressed in dB/m and is written as:

$$\alpha = 1.69\frac{\sigma_e}{\sqrt{\varepsilon_r}} \tag{2}$$

where σ_e is the effective electric conductivity of the site

Table 1 gives order of magnitude of permittivity of some materials.

Table 1. Order of magnitude of permittivity of some materials [27].

Matérials	Permittivity
Clays (*)	8 - 12
Basalt/Andesite	5 - 7
Dry limestone (*)	6 - 8
Granites (*)	5 - 6.5
Sandstone (*)	4 - 5
Quartzites (*)	4 - 5
Sands	4 - 6
Sands saturated with fresh water	30
Salt	5 - 6
Ice cream	3.2
Fresh water	81
Seawater	77
Asphalt/Bitumen	3 - 6
Concrete/Masonry	4 - 12 variable

(*) Natural rock conditions saturated with formation water.

Short electromagnetic waves pass through pavement layers and reflect surfaces or objects that exhibit discontinuities in dielectric properties. Variations in dielectric properties are related, for example, to differences between materials, changes in moisture content or changes in density [28]. The intensity of the reflected pulses is directly proportional to the contrast of dielectric properties between adjacent materials. The reflected pulses are received by the antenna and recorded as waves that are digitized and interpreted by calculating the amplitude and arrival times of each main reflection.

After the GPR method, MASW method is explained.

3. MASW

Surface wave measurements have been continuously improved and have proved useful for roadway testing [6] [7]. In soil mechanics and pavement design, models of materials based on the results of surface wave measurements are beginning to be developed [29] [30] [31] [32]. However, difficulties related to the measurement procedure in pavement seismic testing are always reported.

Today, the MASW method allows an acquisition similar to conventional seismic with the use of several geophones. MASW methods are based on the dispersive nature of surface waves in a layered medium and can be divided into 7 steps (**Figure 1**). It is often accepted that Rayleigh waves are the predominant waves in sub-surface prospecting, with a penetration depth of about one wavelength [33]. However, this assertion is only valid in a medium where stiffness increases

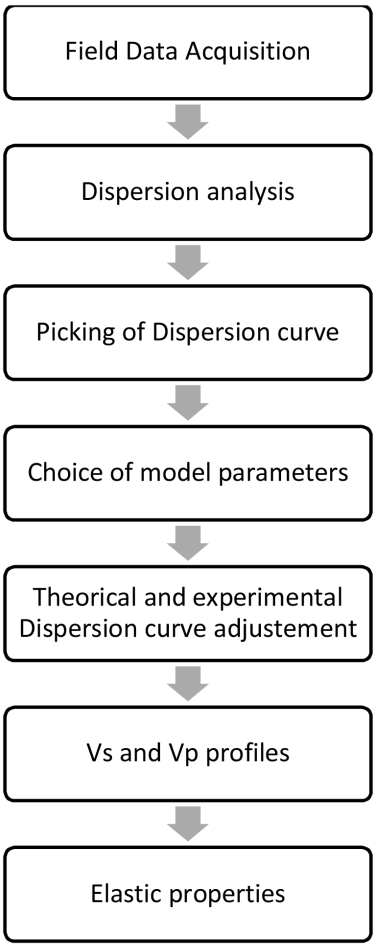

Figure 1. MASW method process.

with depth [34] [35]. In a medium with an inverted velocity profile (*i.e.* stiffness decreases with depth) as with road structures, the nature of the propagation of surface waves is more complex. Many studies have shown that the dispersion curve with phase velocity increasing with frequency (*i.e.* an inverted dispersion curve) is constructed by considering small portions of the higher modes [36] [37] [38]. The MASW approach is thus summed up in a measurement of the experimental dispersion curve of the pavement body and subsequently, define a soil model allowing to find a compromise between the theoretical and experimental dispersion curves, which will make it possible to obtain the variation of the shear velocities of the layers.

The methodology adopted including GPR and MASW is discussed in Section 4.

4. Material and Method

The Radar and MASW measurements were made on a road located inside the Campus of the University of Thies with the following UTM coordinates: −16.960050E and 14.791811N.

First we created a 2D GPR profile. In a second step, we made 1D MASW profiles spaced by 0.2 m in the perpendicular direction and centered on the intersection with the radar profile (Figure 2). 1D MASW profiles are later combined to obtain a 2D MASW profile overlaid with the 2D Radar profile.

For Radar prospecting, the used equipment is a GSSI Radar Structure Scan. It consist of a SIR 3000 connected to an antenna of 1.6 GHz central frequency (cart model 614) (Figure 3).

The radar measurements were carried out in reflection mode which directly provides geometric information.

The permittivity can be calculated according to the reflection amplitudes method [18].

For the paving layer, the relative permittivity is calculated by comparing the amplitude of the reflection on the road surface to the reflection on a metal plate.

$$\varepsilon_1 = \left(\frac{1+\rho_0}{1-\rho_0}\right)^2 \tag{3}$$

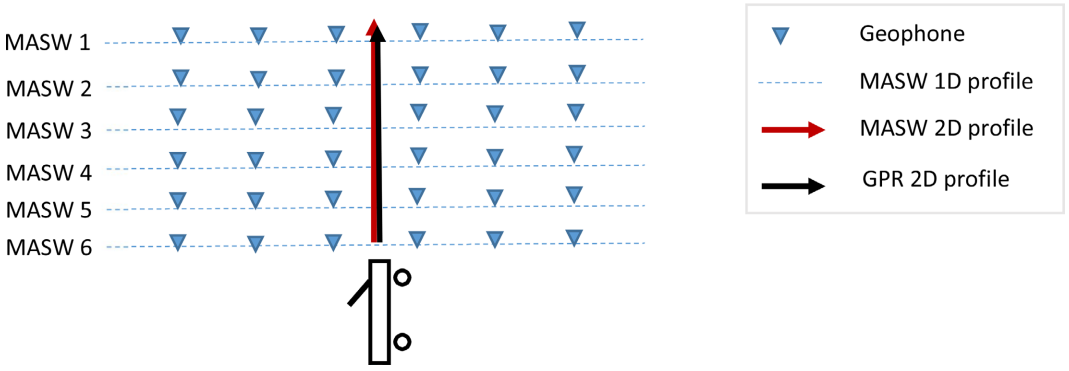

Figure 2. Layout of GPR, MASW 1D and MASW 2D profiles.

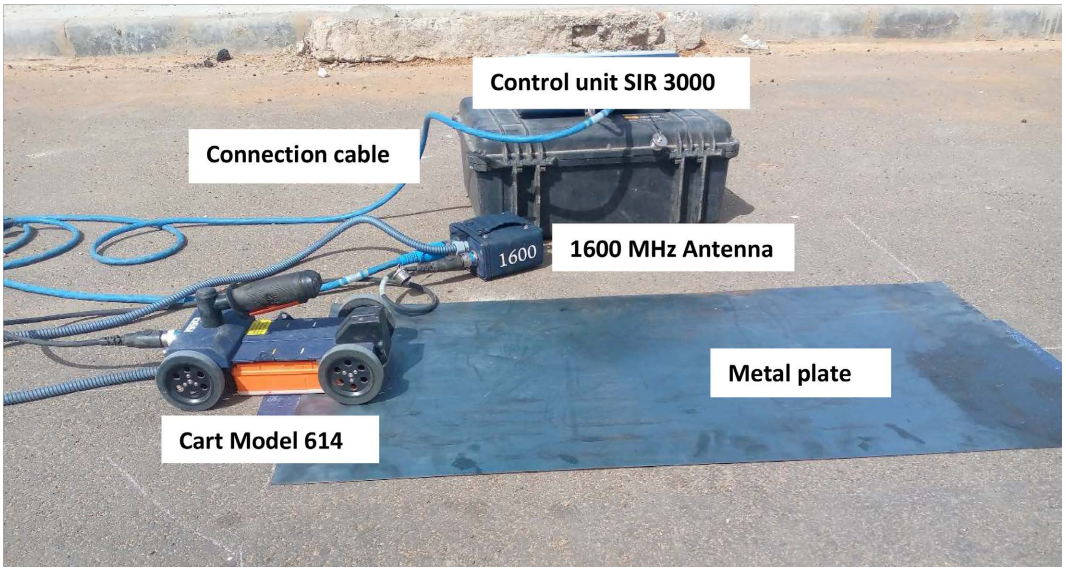

Figure 3. GPR data acquisition with the Radar Structure Scan.

where ε_1 : dielectric constant of the first layer.

With

$$\rho_0 = \frac{A_0}{A_m} \tag{4}$$

A_0: Amplitude of reflection between air and first layer.

A_m: The amplitude of the reflection between the air and a metal plate placed on the pavement.

For the second layer, the relative permittivity can be calculated, but in a slightly more complicated way. We have:

$$\varepsilon_1 = \left(\frac{1+\rho_0^2+\rho_1}{1-\rho_0^2-\rho_1}\right)^2 \tag{5}$$

where ε_2 : diélectric constant of the second layer.

With

$$\rho_1 = \frac{A_1}{A_m} \tag{6}$$

A_1: The amplitude of the reflection at the interface between layer 1 and layer 2.

Finally, for the third layer, the relative dielectric permittivity is calculated as follows:

$$\varepsilon_3 = \varepsilon_2\left(\frac{1+\rho_0^2+\gamma_1\rho_1+\rho_2}{1-\rho_0^2+\gamma_1\rho_1-\rho_2}\right)^2 \tag{7}$$

where ε_3 : dielectric constant of the third layer.

With

$$\rho_2 = \frac{A_2}{A_m} \tag{8}$$

A_2: The amplitude of the reflection at the interface between layer 1 and layer 2

With

$$\gamma_1 = \frac{\sqrt{\varepsilon_1}-\sqrt{\varepsilon_2}}{\sqrt{\varepsilon_1}+\sqrt{\varepsilon_2}} \tag{9}$$

For the MASW survey, a seismograph was developed (**Figure 4**) consisting of an Arduino Due [39] microcontroller connected to a Raspberry Pi 4 nanocomputer [40]. The Raspberry is used as a real-time data acquisition and visualization interface, while the Arduino acts as an analog-to-digital converter. These receivers are made up of six GD 4.5 Hz geophones connected to each other by a graduated ribbon allowing to control the inter-trace distance and faster acquisition of data in land streamer mode. The recording is triggered by a KY-038 sensor [12].

More details about acquisition parameters are given to **Table 2**.

Figure 5 presents a schematic diagram of the combination of MASW and GPR methods.

Obtained results will be discussed in the following section.

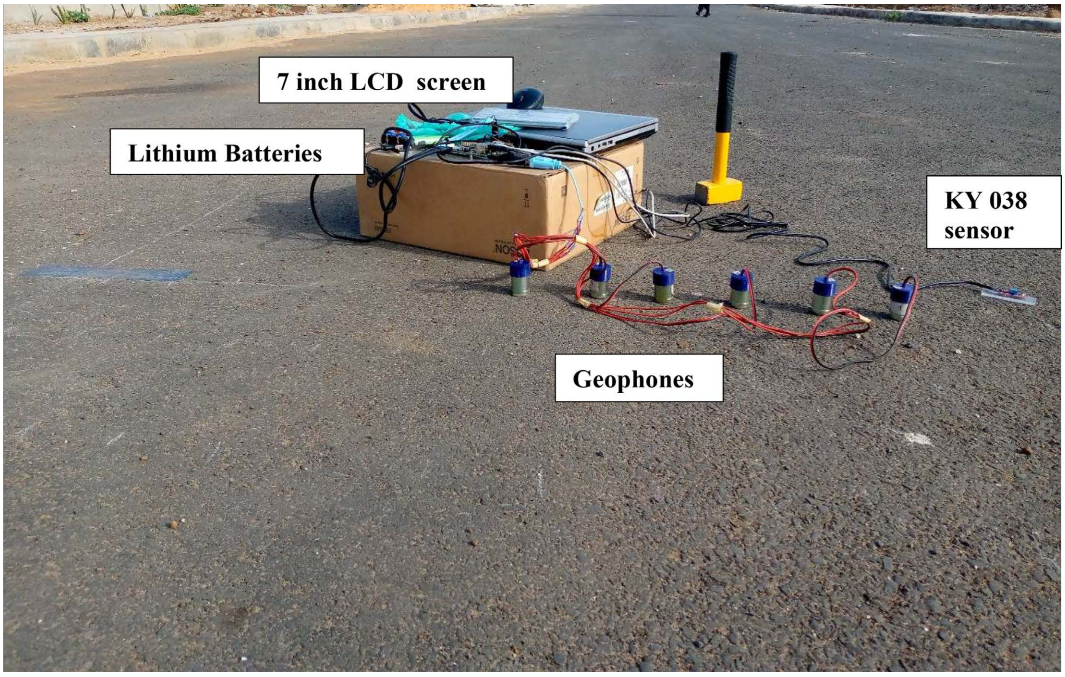

Figure 4. MASW data acquisition on pavement.

Table 2. Acquisition parameters.

Source	Marteau de 1 Kg
Offset	0.5 m
Geophone	Vertical 4.5 Hz
Distance between geophones	0.1 m
Number of Geophones	6
Sampling interval	4×10^{-6} s
Measuring time	0.008 s
Number of samples	2000
Sampling frequency	250,000

5. Results and Discussions

Raw Radar data are shown in Figure 5.

An important step in processing is the profile time to depth conversion. This requires knowledge of the propagation velocities of the investigated materials. The rate of propagation can be easily estimated from Equation (1) where permittivities are obtained by exploiting Equations (3), (5), (7). The amplitudes at the different interfaces obtained on the radargrams are recorded in Table 3. The velocities obtained are presented in Table 4.

From velocities in Table 4, we can convert the time axis to depth (Figure 6).

After identifying the different interfaces between the layers, the thicknesses can be read directly on the vertical axis on the right (Table 5).

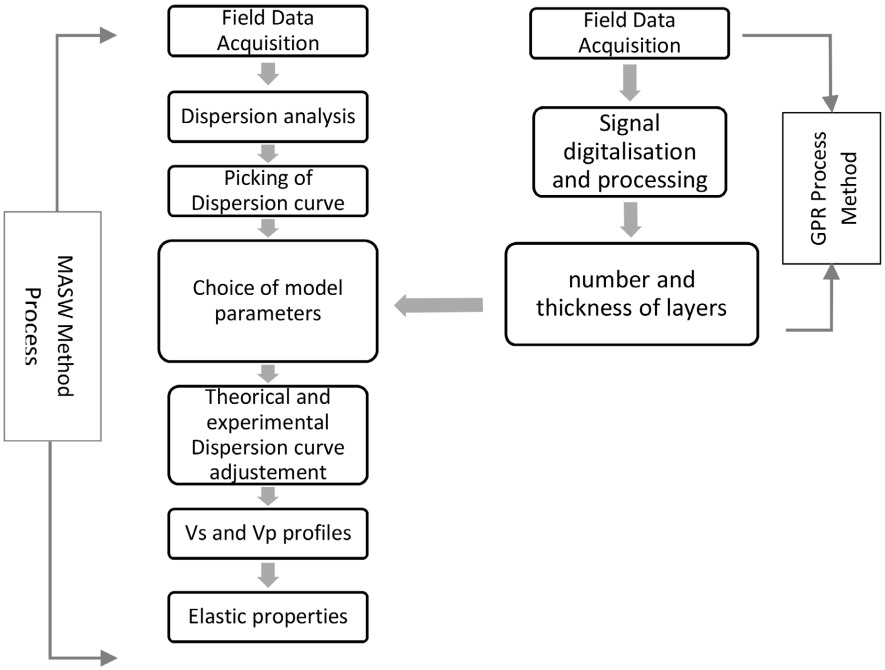

Figure 5. Schematic diagram of the combination of MASW and GPR methods.

Table 3. Amplitudes and permittivities of the different layers of the pavement (A_0: air/pavement interface, A_1: base bearing interface, A_2: base/platform interface, Am: amplitude on the metal plate).

Distance (m)	Amplitudes				γ	ε_1	ε_2	ε_3
	A_m	A_0	A_1	A_2	**−0.29**	**9.34**	**17.17**	**20.88**
0	3427	6760	9363	60	−0.34	11.64	23.00	26.40
0.2	3645	6667	9427	228	−0.18	5.27	7.89	9.90
0.4	2868	7293	10,048	58	−0.28	8.55	15.45	19.50
0.6	3435	7007	9081	250	−0.25	7.19	12.16	15.53
0.8	3264	7148	9319	148	−0.32	10.59	20.15	23.49
1	3198	6035	8671	130	−0.29	9.34	17.17	20.88

Table 4. Radar velocity of different layers.

Distance (m)	0	0.2	0.4	0.6	0.8	1
Paving velocity (m/ns)	0.098	0.088	0.010	0.012	0.012	0.092
Base layer velocity (m/ns)	0.072	0.063	0.076	0.086	0.086	0.066
Platform Velocity (m/ns)	0.066	0.058	0.068	0.076	0.076	0.061

Table 5. Thickness of layers.

Layers	Thickness (cm)	Depth (cm)
Paving layer	3.5	0
Base layer	7.5	−3.5
Platform layer	20	−7.5

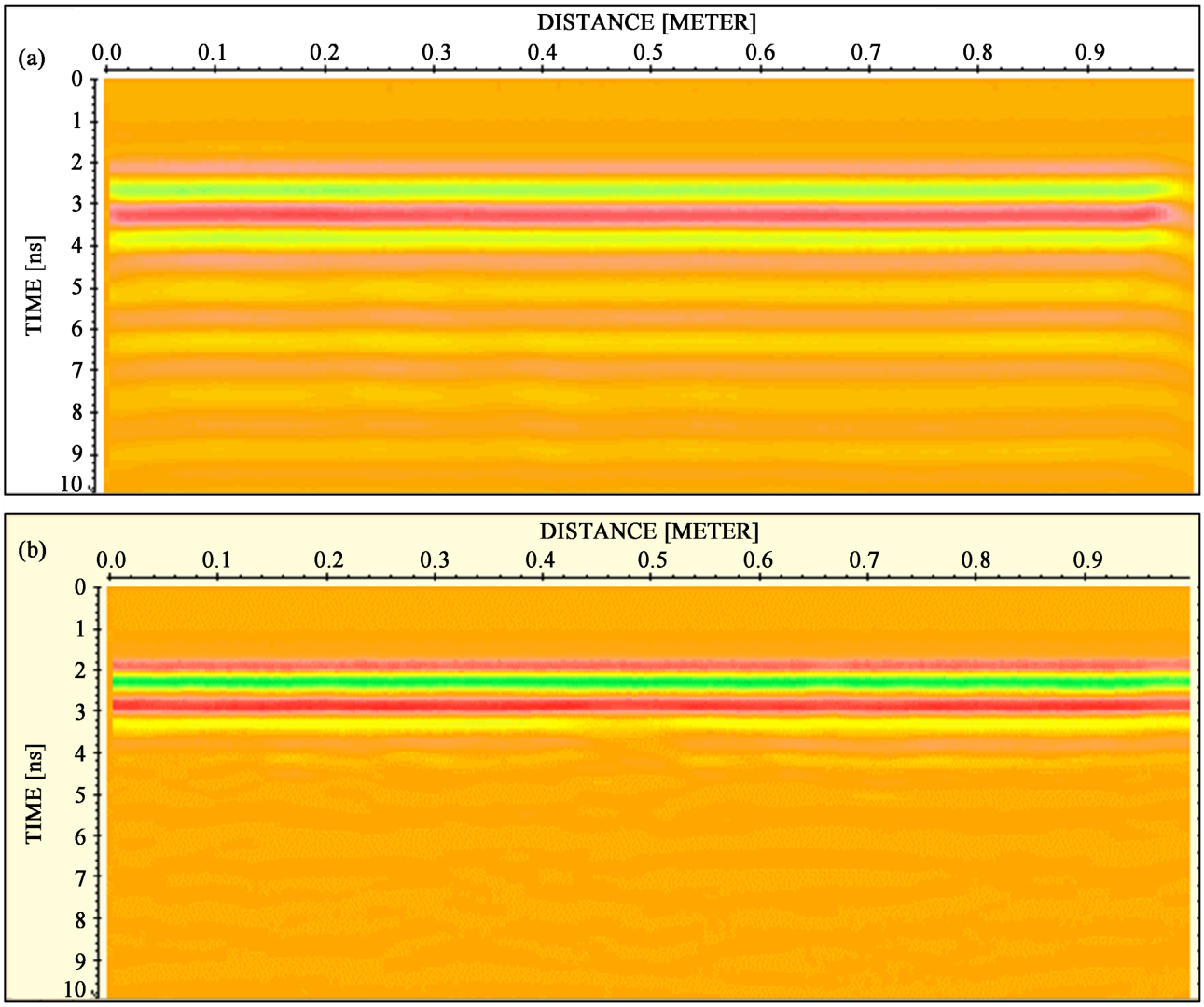

Figure 6. Raw radar data with metal plate (a) and without metal plate (b).

The MASW data are displayed using the Open Source Geopsy software [40] as a seismogram (**Figure 7**).

In order to assess the energy range within which an interpretation of the results is possible, we carried out a dispersion analysis (**Figure 8**). This step with the Geopsy [40] software is performed by introducing the geometry of the MASW profile and applying a linear FK analysis with velocity ranges in the range [0, 1000], and frequency in the interval [0, 800] and a linear sampling step of 100 is applied for both velocity and frequency.

Figure 9 shows a maximum energy between approximately 70 Hz and 200 Hz, corresponding to the fundamental mode, indicating the desired dispersion curve. The dispersion is reversed compared to a normal situation where low frequencies propagate at higher velocities. This reversal is explained by the decrease of velocities with the depth on the pavements. This interval [70 - 200] was confirmed by the work of Park (2018) which showed that it is dependent on the length of the

profile and the spread of the geophones. These results are also confirmed at various sites studied by Diene and Ndiaye (2022) with the same acquisition device.

The experimental dispersion curve is then extracted to allow data inversion.

The inversion is done using the integrated Dinver module of Geopsy. The first step is the selection of model parameters including a priori knowledge (Ólafsdóttir, 2016). The layer thicknesses obtained with the Radar auscultation results and

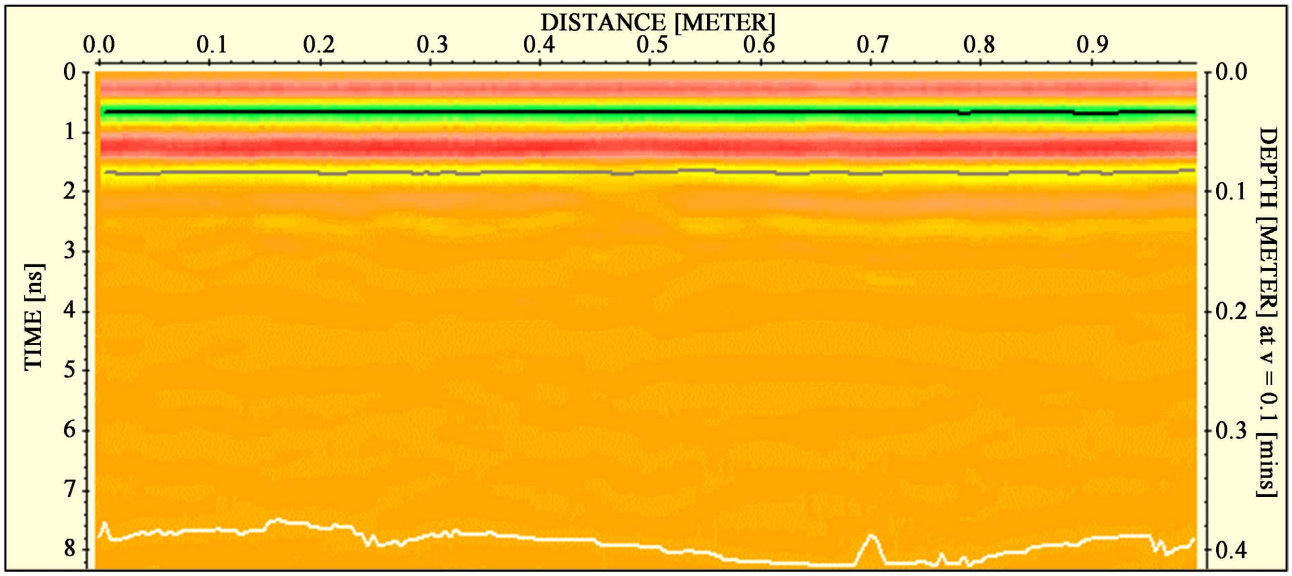

Figure 7. Radar profile as a function of depth.

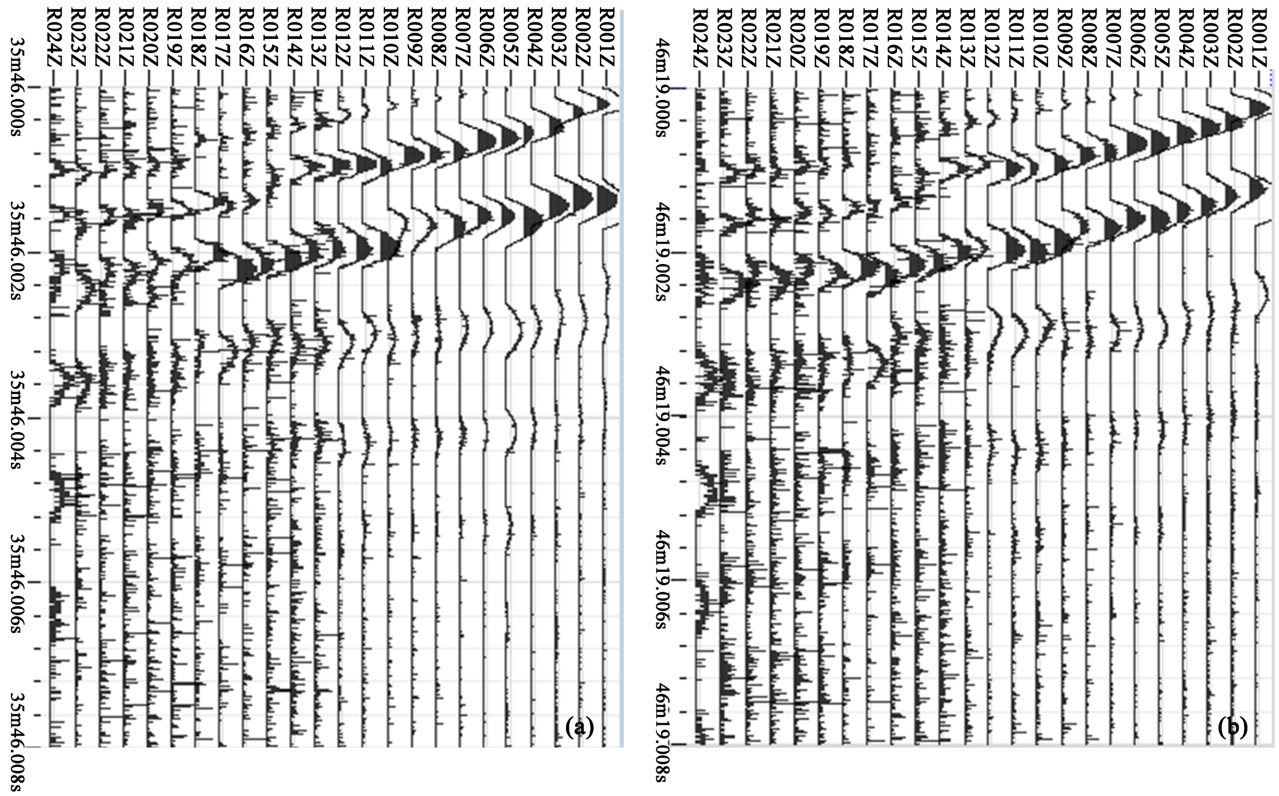

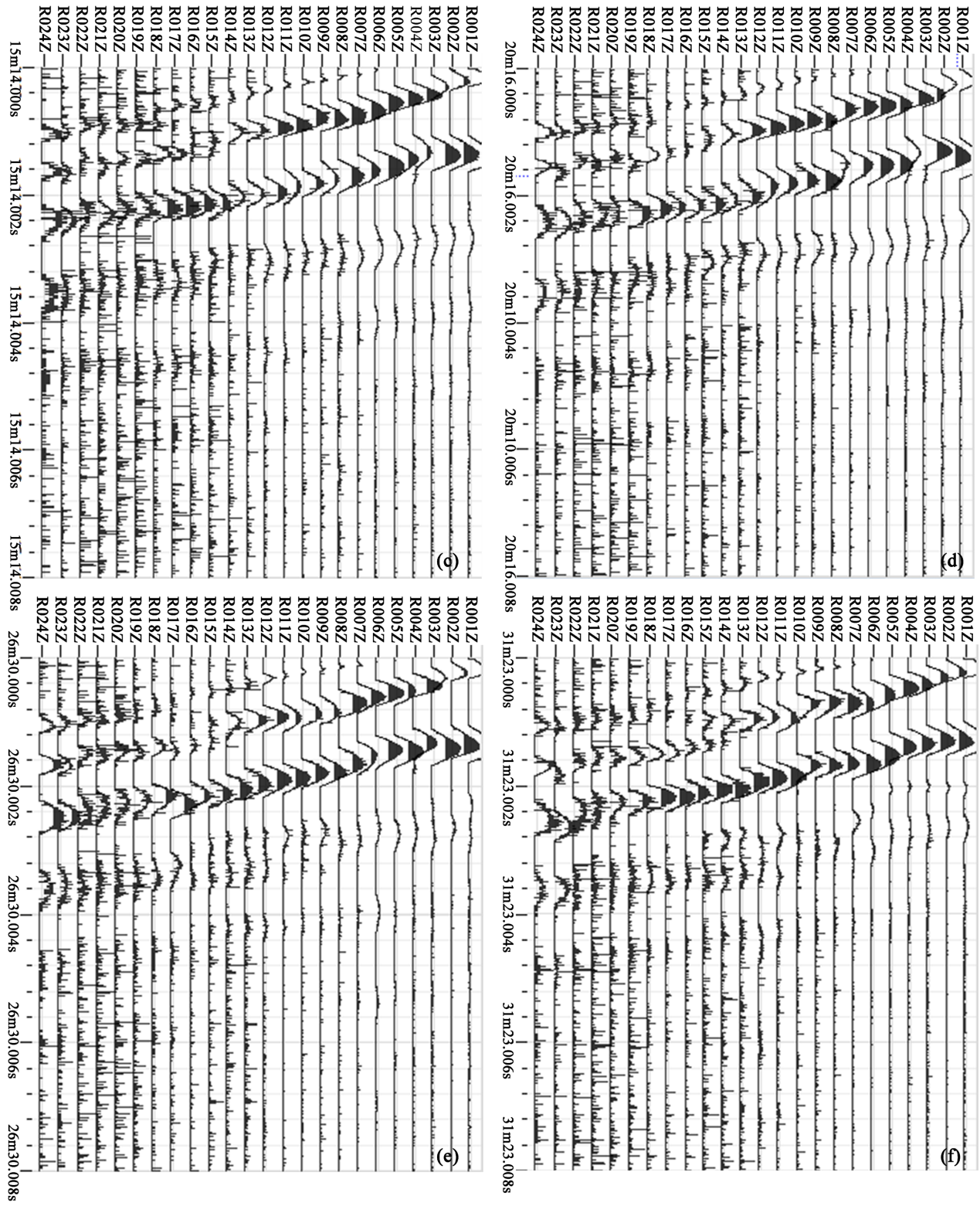

Figure 8. The Seismograms of the six 1D MASW profiles: MASW1 (a); MASW 2 (b); MASW 3 (c); and MASW 4 (d); MASW 5 (e); MASW 6 (f).

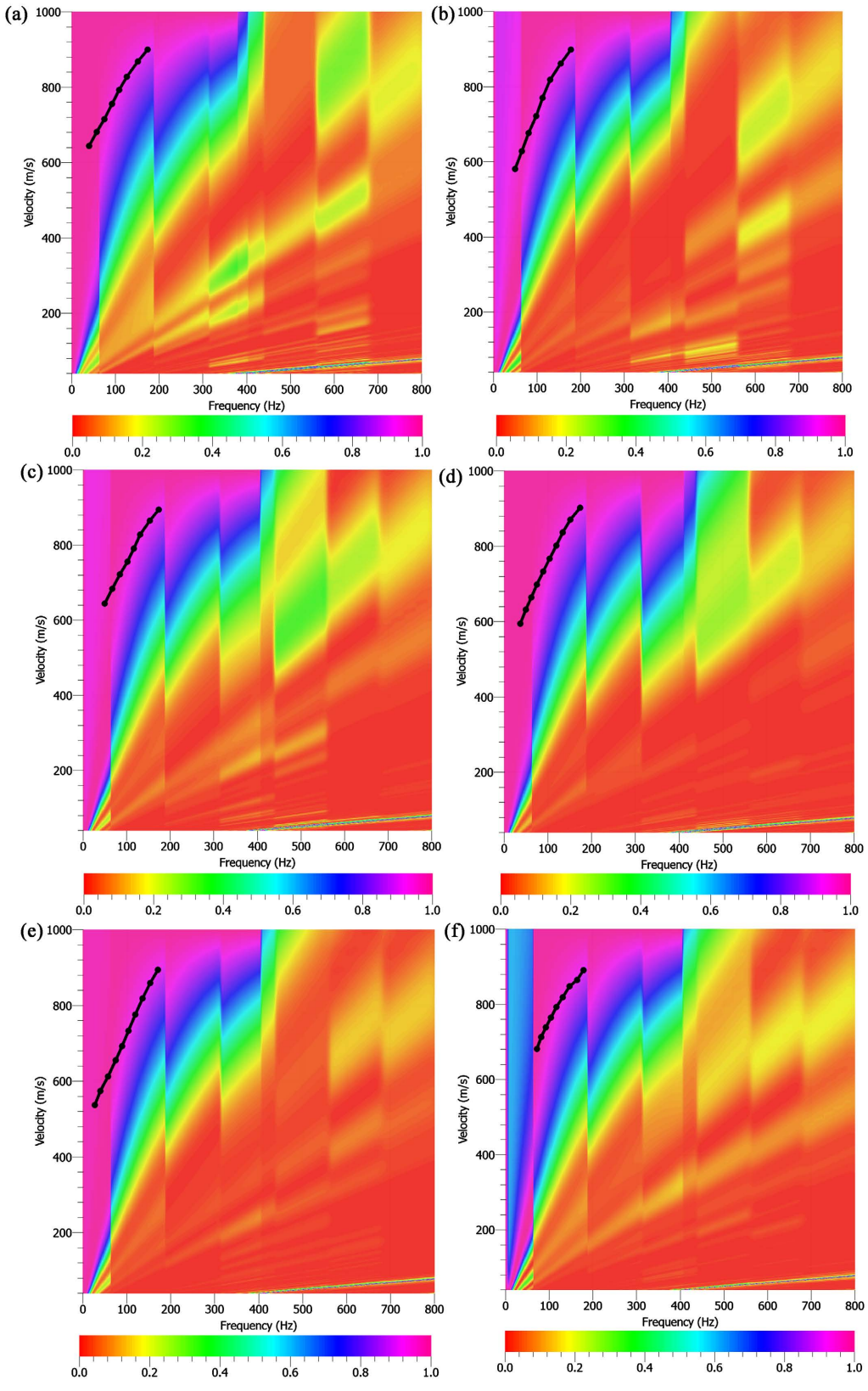

Figure 9. Dispersion curves: MASW1 (a); MASW 2 (b); MASW 3 (c); and MASW 4 (d); MASW 5 (e); MASW 6 (f).

presented in section 5.2 gives the model thicknesses that will be fixed.

The quality of the inversion, the number of iterations, the convergence and the misfit are available on log files. The inversion gives very low misfits values (less than 1%) after a 50 iterations. The good superposition between the theoretical and experimental dispersion curves (Figure 10) confirms the quality of the model obtained after inversion.

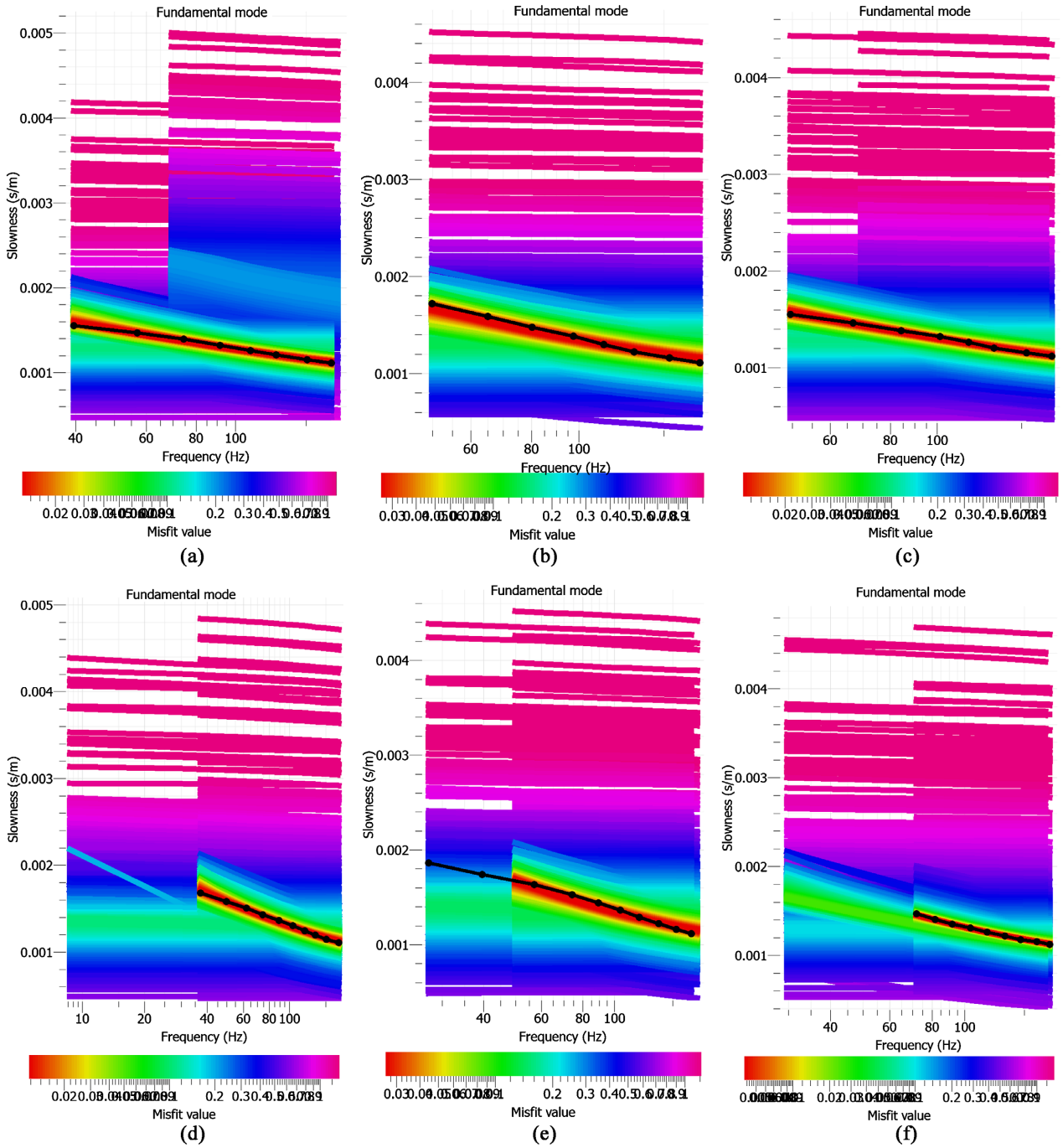

Figure 10. Overlay of theoretical and experimental dispersion curves: MASW1 (a); MASW 2 (b); MASW 3 (c); and MASW 4 (d); MASW 5 (e); MASW 6 (f).

The velocity profiles for the investigated sites are shown in Figure 10.

From the data in Figure 11 showing the variations in V_P and V_S velocities, it is

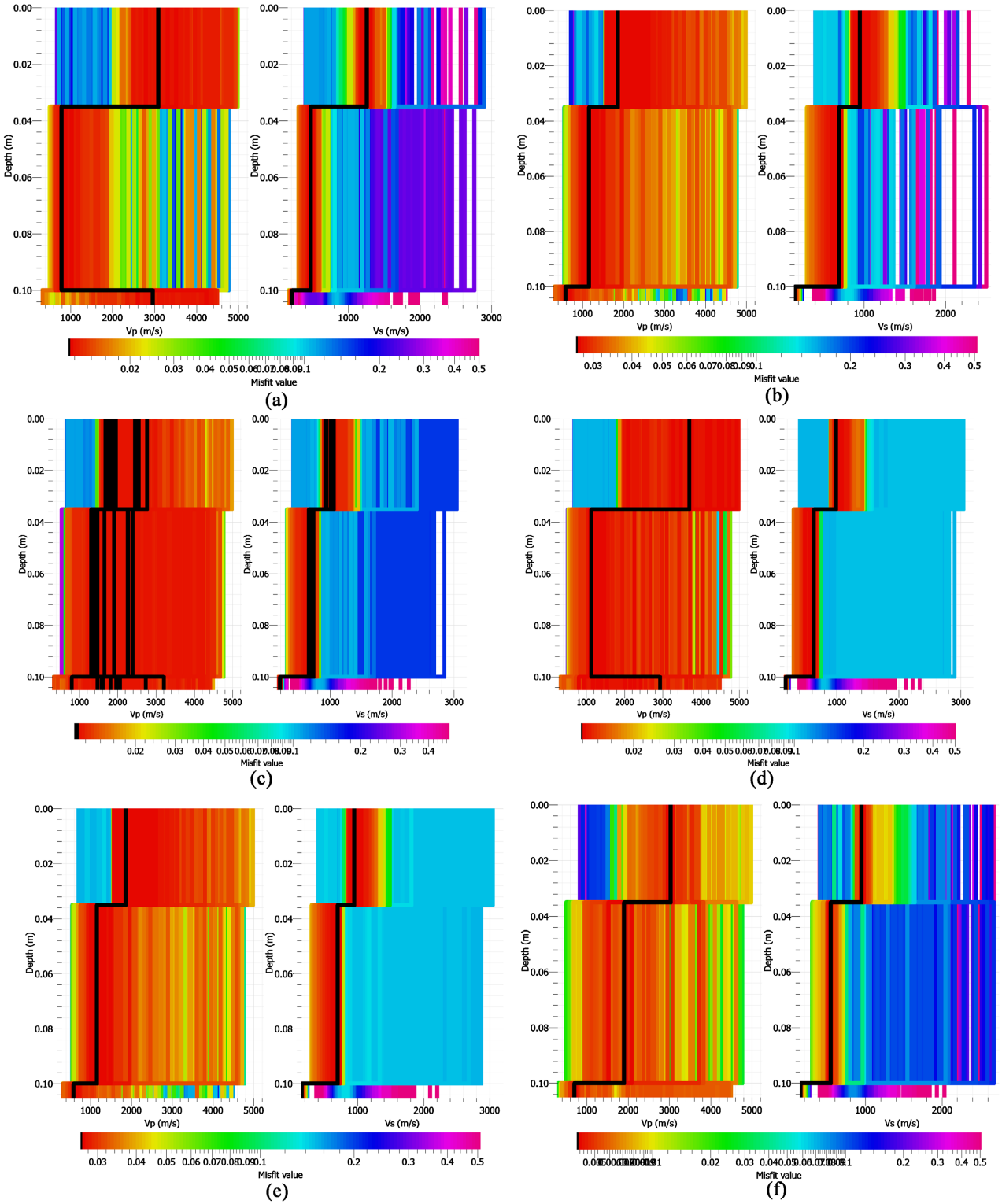

Figure 11. V_P and V_S profiles obtained by inversion: MASW1 (a); MASW 2 (b); MASW 3 (c); MASW 4 (d); MASW 5 (e); MASW 6 (f).

possible to summarise the MASW data according to the position in the 2D profile (Table 6).

Using the MASW (Table 6) and GPR (Table 4) data, we reconstructed the pavement profile using the velocities V_P, V_S and V_{GPR} (Figures 12(a)-(c)).

The V_S profile, shows that the velocities are maximum (above 850 m/s) in the paving layer. Velocities of 650 to 850 m/s are encountered in the base layer and the lowest velocities (150 to 650 m/s) in the platform.

On the V_P profile, the velocities are high (above 2400 m/s) in the paving layer, moderately high in the base layer (1800 to 2400 m/s) and lower in the platform (below 1800 m/s).

On the radar profile, the velocities are also higher in the paving layer (above 0.09 m/ns) moderately high in the base layer (0.08 to 0.09 m/ns) and lower in the platform (below 0.08 m/ns)

The Vs velocities have an almost homogeneous distribution in the paving layer and platform. They show some heterogeneities in the base layer. The V_P velocities show heterogeneities in the three layers (paving, base and platform). The heterogeneities are most pronounced in the paving layer in the distance intervals [0.1; 0.25] and [0.75; 0.85]. In the base layer, heterogeneities are mainly noted in the distance intervals [0.55; 0.65]. Radar velocities show heterogeneities in the three layers in the distance intervals [0.15; 0.25] and [0.5; 0.9]. Basically, the heterogeneities are noted and more marked according to the profiles in two zones: zone 1 in the range [0.1; 0.25] and zone 2 in the range [0.5; 0.9]

In zone 1 [0.1; 0.25] the heterogeneities appear well on the V_P and V_{GPR} profiles and a little less on the Vs profile. The decrease of V_P and V_{GPR} is noted, on the other hand we have a slight decrease then an increase of Vs. The decrease in V_P could be due to a decrease in mechanical properties by a decrease in compactness. This hypothesis can be supported by the decrease in V_{GPR} due to a higher water content in voids, and the local decrease in Vs due to the difficulty of shear waves to propagate in a wetter environment.

Table 6. V_S and V_P according to the depth and position of the profile

Depth (m) \ Distance (m)	0	0.2	0.4	0.6	0.8	1
0 - 0.035	3050	1850	2750	3700	1850	3000
0.035 - 0.1	800	1200	1900	1100	1200	1900
10	2950	600	900	1900	650	700

Depth (m) \ Distance (m)	0	0.2	0.4	0.6	0.8	1
0 - 0.035	1250	950	1000	950	950	980
0.035 - 0.1	450	700	750	600	700	580
10	200	180	200	180	180	180

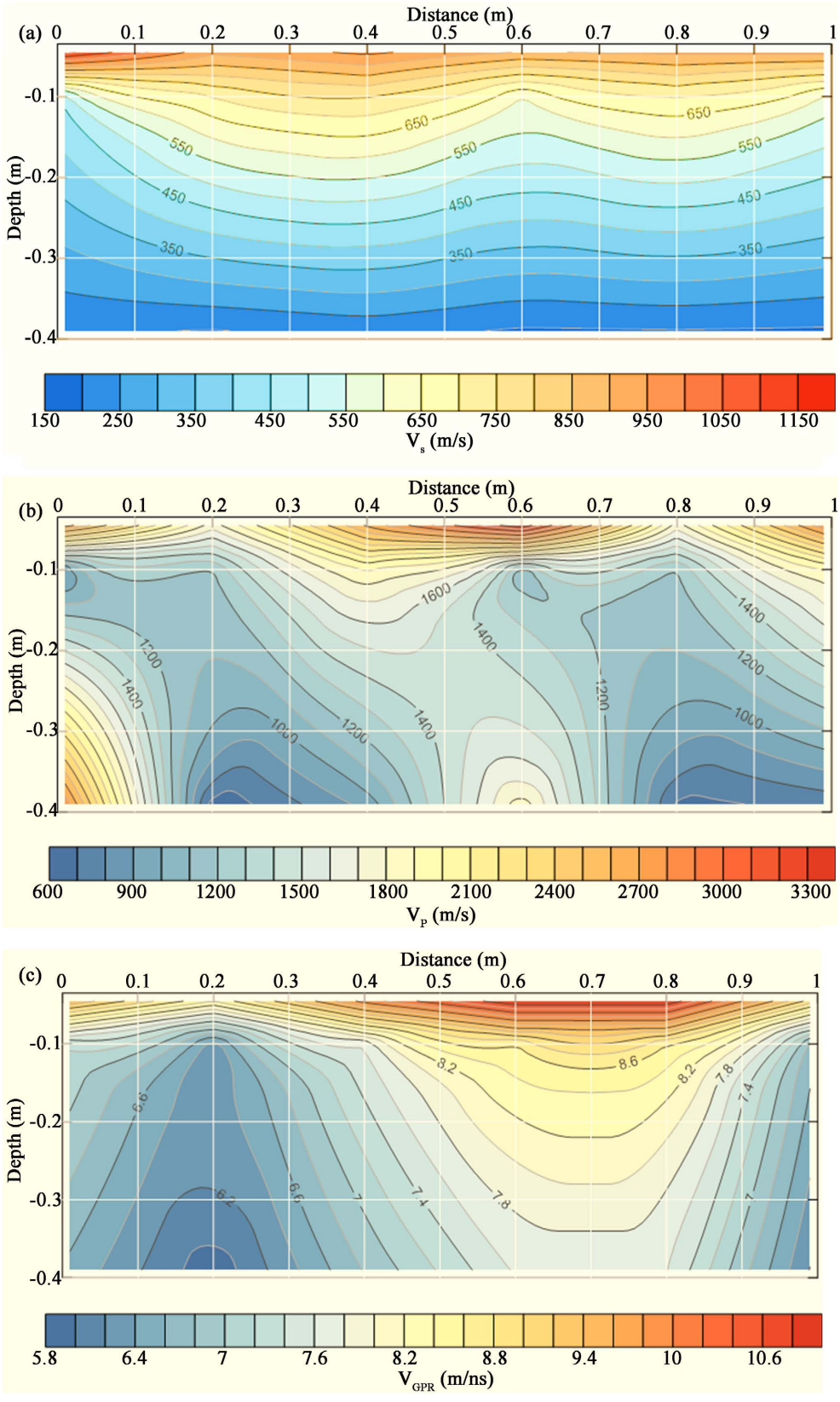

Figure 12. Reconstruction of the pavement using V_S (m/s) (a), V_P (m/s) (b) and V_{GPR} (m/ns) (c) velocities.

In zone 2 [0.5; 0.9], we generally note an increase in V_S and V_{GPR}, but we note a decrease in V_P. This could be related to the presence of dry voids.

Based on Figure 11, it should also be added that the MASW method used is more sensitive to V_S variations than to V_P variations due to single value of V_S obtained after inversion. The elastic modules can be estimated from 5300 to 9800 MPa in the bearing layer and from 3100 to 5300 MPa in the base layer.

6. Conclusions

The integration of the number of layers and thicknesses obtained from radar data makes it possible to obtain more precise V_S and V_P profiles from the MASW method. Indeed, these data allow to reduce the inversion parameters.

The obtained profiles show that all velocities decrease with depth. In the case of seismic data, the velocity decreases are due to a decrease in mechanical properties as we move from the paving layer to the base layer and platform. In the case of radar waves, the decrease in velocity is mainly explained by the decrease in water content. The hydrophobic nature of the bitumen in the paving layer, the optimum Proctor compaction of the base layer and the presence of natural water contents in the subgrade could explain this increase in water contents.

The heterogeneities that appear simultaneously on the V_P and V_{GPR} profiles appear to be related to water-saturated voids, while those that appear on both the V_S and V_{GPR} profiles would be due to dry voids.

Radar waves propagate in the road layers at velocities almost 2×10^5 times higher than S waves and more than 6×10^4 times higher than P waves. This large difference in velocity is explained by the fact that radar waves are electromagnetic waves propagating by moving electric charges as seismic waves move matter.

Further investigation is needed to understand the role of relative orientation between MASW and GPR profiles in observed heterogeneities.

Conflicts of Interest

The authors declare no conflicts of interest regarding the publication of this paper.

References

[1] Towada, B.T.M. and Assaf, G.J. (2016) Intégration de la cause de détérioration des routes en afrique subsaharienne/integration of the cause of deterioration of roads in sub-saharan africa. *Annales du Bâtiment et des Travaux Publics*, **68**, 27.

[2] Makhaly, B., Tinjum, J.M. and Fall, M. (2015) Prediction of Permanent Deformation Model Parameters of Unbound Base Course Aggregates under Repeated Loading. *Road Materials and Pavement Design*, **16**, 854-869. https://doi.org/10.1080/14680629.2015.1063534

[3] Jones, R. (1962) Surface Wave Technique for Measuring the Elastic Properties and Thickness of Roads: Theoretical Development. *British Journal of Applied Physics*, **13**, 21. https://doi.org/10.1088/0508-3443/13/1/306

[4] Nazarian, S. and Stokoe, K.H. (1985) *In Situ* Determination of Elastic Moduli of

Pavement Systems by Spectral-Analysis-of-Surface-Waves Method: Practical Aspects.

[5] Nazarian, S., Stokoe II, K.H. and Hudson, W.R. (1983) Use of Spectral Analysis of Surface Waves Method for Determination of Moduli and Thicknesses of Pavement Systems. No. 930.

[6] Nazarian, S. (1984) In Situ Determination of Elastic Moduli of Soil Deposits and Pavement Systems by Spectral-Analysis-of-Surface-Waves Method (Shear Velocity, Propagation, Liquefaction, Non-Destructive, Earthquake). Diss., The University of Texas, Austin.

[7] Aouad, M.F. (1993) Evaluation of Flexible Pavements and Subgrades Using the Spectral-Analysis-of-Surface-Waves (SASW) Method. Diss., The University of Texas, Austin.

[8] Rydèen, N. (2004) Surface Wave Testing of Pavements. 47.

[9] Suto, K. (2014) Use of an MASW Survey to Assess Flood Damaged Road—A Case History. 27*th Annual Symposium on the Application of Geophysics to Engineering and Environmental Problems* (*SAGEEP*), Boston, 16-20 March 2014, 7.

[10] Lin, S. and Ashlock, J.C. (2015) Comparison of MASW and MSOR for Surface Wave Testing of Pavements. *Journal of Environmental and Engineering Geophysics*, **20**, 277-285. https://doi.org/10.2113/JEEG20.4.277

[11] Park, C., Richter, J., Rodrigues, R. and Cirone, A. (2018) MASW Applications for Road Construction and Maintenance. *The Leading Edge*, **37**, 724-730. https://doi.org/10.1190/tle37100724.1

[12] Diene, C. and Ndiaye, M. (2022) Design and Application of a Multichannel Analysis Surface Waves Acquisition System for the Pavement Layers Investigation. *Open Journal of Civil Engineering*, **12**, 22-37. https://doi.org/10.4236/ojce.2022.121003

[13] Al-Qadi, I.L. and Lahouar, S. (2004) Use of GPR for Thickness Measurement and Quality Control of Flexible Pavements. *Journal of the Association of Asphalt Paving Technologists*, **73**, 501-528.

[14] Li, X.T., Wang, D.-Y. and Zhang, X.-N. (2006) A High-Accuracy Calibration Method for Thickness Measurements of Asphalt Pavement Using Ground Penetrating Radar. 25*th Annual Southern African Transport Conference*, Pretoria, 10-13 July 2006, 305-312.

[15] Maser, K. and Vandre, B. (2006) Network-Level Pavement Structure Assessment Using Automated Processing of Ground Penetrating Radar (GPR) Data. *Airfield and Highway Pavements Specialty Conference*, Atlanta, 30 April-3 May 2006, 719-728. https://doi.org/10.1061/40838(191)61

[16] Muller, W. and Dérobert, X. (2013) A Comparison of Phase-Shift and One-Port Coaxial Cell Permittivity Measurements for GPR Applications. 7*th International Workshop on Advanced Ground Penetrating Radar*, Nantes, 2-5 July 2013, 1-6. https://doi.org/10.1109/IWAGPR.2013.6601526

[17] Shang, J.Q., *et al.* (1999) Measurement of Complex Permittivity of Asphalt Pavement Materials. *Journal of Transportation Engineering*, **125**, 347-356. https://doi.org/10.1061/(ASCE)0733-947X(1999)125:4(347)

[18] Maser, K.R., Scullion, T. and Briggs, R.C. (1991) Use of Radar Technology for Pavement Layer Evaluation. NASA STI/Recon Technical Report N 93, 21744.

[19] Topp, G.C. and Davis, J.L. (1981) Detecting Infiltration of Water through Soil Cracks by Time-Domain Reflectometry. *Geoderma*, **26**, 13-23. https://doi.org/10.1016/0016-7061(81)90073-2

[20] Samui, P. (2014) Utilization of Gaussian Process Regression for Determination of Soil Electrical Resistivity. *Geotechnical and Geological Engineering*, **32**, 191-195. https://doi.org/10.1007/s10706-013-9705-8

[21] Stoffregen, H., Zenker, T. and Wessolek, G. (2002) Accuracy of Soil Water Content Measurements Using Ground Penetrating Radar: Comparison of Ground Penetrating Radar and Lysimeter Data. *Journal of Hydrology*, **267**, 201-206. https://doi.org/10.1016/S0022-1694(02)00150-6

[22] Saarenketo, T. and Scullion, T. (2000) Road Evaluation with Ground Penetrating Radar. *Journal of Applied Geophysics*, **43**, 119-138. https://doi.org/10.1016/S0926-9851(99)00052-X

[23] Zenone, T., *et al.* (2008) Preliminary Use of Ground-Penetrating Radar and Electrical Resistivity Tomography to Study Tree Roots in Pine Forests and Poplar Plantations. *Functional Plant Biology*, **35**, 1047-1058. https://doi.org/10.1071/FP08062

[24] Surette, E., Barnes, C. and Ali, N. (2014) Paper 1: Use of GPR and MASW to Complement Backcalculated Moduli and Design Life Calculations. *In-Situ* Asphalt Master Curve Construction Using Non-Destructive Testing Techniques. 10.

[25] Loizos, A. and Plati, C. (2007) Accuracy of Pavement Thicknesses Estimation Using Different Ground Penetrating Radar Analysis Approaches. *NDT & e International*, **40**, 147-157. https://doi.org/10.1016/j.ndteint.2006.09.001

[26] Harari, Z. (1996) Ground-Penetrating Radar (GPR) for Imaging Stratigraphic Features and Groundwater in Sand Dunes. *Journal of Applied Geophysics*, **36**, 43-52. https://doi.org/10.1016/S0926-9851(96)00031-6

[27] Plati, C. and Loizos, A. (2013) Estimation of *In-Situ* Density and Moisture Content in HMA Pavements Based on GPR Trace Reflection Amplitude Using Different Frequencies. *Journal of Applied Geophysics*, **97**, 3-10. https://doi.org/10.1016/j.jappgeo.2013.04.007

[28] Heukelom, W. (1961) Analysis of Dynamic Deflexions of Soils and Pavements. *Geotechnique*, **11**, 224-243. https://doi.org/10.1680/geot.1961.11.3.224

[29] Omar, M.N., *et al.* (2011) Prediction of Long-Term Settlement on Soft Clay Using Shear Wave Velocity and Damping Characteristics. *Engineering Geology*, **123**, 259-270. https://doi.org/10.1016/j.enggeo.2011.06.004

[30] Heukelom, W., Klomp, A.J.G. and Niesman, T.W. (1968) An Improved Mobile Unit for the Dynamic Testing of Pavements. *Journal of Physics E: Scientific Instruments*, **1**, 127. https://doi.org/10.1088/0022-3735/1/2/310

[31] Aouad, M.F. (1993) Evaluation of Flexible Pavements and Subgrades Using the Spectral-Analysis-of-Surface-Waves (SASW) Method. Diss., The University of Texas, Austin.

[32] Ekdahl, U., Grundteknik, P. and Peab Sverige, A.B. (2004) Quality Control of Cement Stabilised Soil Using Non-Destructive Seismic Tests.

[33] Xu, C.Q. and Butt, S.D. (2006) Evaluation of MASW Techniques to Image Steeply Dipping Cavities in Laterally Inhomogeneous Terrain. *Journal of Applied Geophysics*, **59**, 106-116. https://doi.org/10.1016/j.jappgeo.2005.08.003

[34] Park, C., *et al.* (2018) MASW Applications for Road Construction and Maintenance. *The Leading Edge*, **37**, 724-730. https://doi.org/10.1190/tle37100724.1

[35] Tran, K.T. and Hiltunen, D.R. (2008) A Comparison of Shear Wave Velocity Profiles from SASW, MASW, and ReMi Techniques. *Geotechnical Earthquake Engineering and Soil Dynamics*, Vol. 4, 1-9. https://doi.org/10.1061/40975(318)56

[36] Tokimatsu, K., Tamura, S. and Kojima, H. (1992) Effects of Multiple Modes on

Rayleigh Wave Dispersion Characteristics. *Journal of Geotechnical Engineering*, **118**, 1529-1543. https://doi.org/10.1061/(ASCE)0733-9410(1992)118:10(1529)

[37] Park, C.B., *et al.* (1999) Higher Mode Observation by the MASW Method. SEG Technical Program Expanded Abstracts 1999. Society of Exploration Geophysicists, Houston, 524-527. https://doi.org/10.1190/1.1821070

[38] Wathelet, M., Chatelain, J.L., Cornou, C., Giulio, G.D., Guillier, B., Ohrnberger, M. and Savvaidis, A. (2020) Geopsy: A User-Friendly Open-Source Tool Set for Ambient Vibration Processing. *Seismological Research Letters*, **91**, 1878-1889. https://doi.org/10.1785/0220190360

[39] Due, A. and Core, A.R.M. (2019) Arduino Due. Retrieved 9.16 (2017).

[40] Richardson, M. and Wallace, S. (2012) Getting Started with Raspberry PI. O'Reilly Media, Inc., Sebastopol.